CGMTorch: A Framework for Gradient-based Design of Computational Granular Metamaterials

Atoosa Parsa [1]   Corey S. O'Hern [2]   Rebecca Kramer-Bottiglio [2]   Josh Bongard [1]

Abstract

Unconventional computing devices leverage the intrinsic dynamics of a physical substrate to perform fast, energy-efficient, and special-purpose computations. Granular metamaterials have great potential for creating such computing devices. However, there is no general framework for the inverse design of large-scale granular materials. Here, we develop a gradient-based optimization framework for harmonically driven granular materials to obtain a target wave response. Using this framework, we design basic logic gates in which mechanical vibrations carry the information at predetermined frequencies. Our findings show that a gradient-based optimization method can greatly expand the design space of computational metamaterials and provide the opportunity to systematically traverse their parameter space to find materials with the desired functionalities.

1. Introduction

Advances in physics, chemistry, and materials science, along with revolutionary fabrication and manufacturing technologies, have provided the opportunity to explore unconventional computing paradigms that abandon the notion of centralized processing units and harness the natural dynamics of the physical system to perform the desired computation. With this perspective, any controllable physical system with rich intrinsic dynamics can be exploited as a computational resource. This has resulted in the development of mechanical (Lee et al., 2022), optical (Anderson et al., 2023), electromechanical (El Helou et al., 2022) and biological (Roberts & Adamatzky, 2022) computing units. Such physics-based computing devices offer potential advantages for fast and efficient computation that avoids analog-to-digital conversion and allows massively parallel operations (Yasuda et al., 2021). However, finding the best hardware setup is often a challenging task beyond the intuitive limits of human experts and can benefit from automatic design methodologies to tune various aspects of the system according to the application (Finocchio et al., 2023).

This paper focuses on the inverse design methodologies for computational metamaterials. Metamaterials are engineered composite materials designed with particular spatial configurations that exhibit macroscopic behaviors different from their constituent parts (Xia et al., 2022). They can possess non-natural static or dynamic properties such as negative bulk moduli and mass density, non-reciprocity, and auxetic behavior (Kadic et al., 2019; Jiao et al., 2023). Mechanical metamaterials, especially those made of field-responsive materials, have received immense attention for robotics applications where they can respond to various stimuli and reconfigure to adapt to different environmental conditions (Rafsanjani et al., 2019). They provide increased robustness and reduced power consumption in the system and enable the design of highly tunable multifunctional mechanisms that integrate sensing, information processing, and actuation in fully autonomous engineered systems (Pishvar & Harne, 2020). The ability to create metamaterials that can manipulate mechanical vibrations of varying frequencies has made them an excellent platform for mechanical computation (Yasuda et al., 2021).

Here, we concentrate on a subset of metamaterials with particulate structures, namely granular materials. These are composite materials made of noncohesive particles with various material properties and shapes, which are densely packed in random or carefully designed configurations (Karuriya & Barthelat, 2023). Due to their discrete nature and the nonlinearity of interparticle contacts, granular materials exhibit highly tunable dynamic responses and are utilized in a broad range of applications, including energy localization and vibration absorption layers (Zhang et al., 2015; Taghizadeh et al., 2021), acoustic computational units like switches and logic elements (Li et al., 2014; Parsa et al., 2023), granular actuators (Eristoff et al., 2022), acoustic filters (Boechler et al., 2011), and sound focusing/scrambling devices (Porter et al., 2015).

[1]Department of Computer Science, University of Vermont, Burlington, VT, USA [2]Department of Mechanical Engineering and Materials Science, Yale University, New Haven, CT, USA. Correspondence to: Atoosa Parsa <atoosa.parsa@gmail.com>.

Granular materials are commonly studied in a confined structure subject to external vibrations. Their nonlinear dynamic response is highly tunable by local changes to individual particles' properties. Therefore, they possess great potential for wave-based physical computation. However, with such high-dimensional parameter space and strongly nonlinear discrete dynamics, tuning their vibrational response is extremely challenging. Many studies are limited to experimental measurements (Boechler et al., 2011; Li et al., 2014; Lawney & Luding, 2014; Cui et al., 2018) or numerical integration of the equations of motion (Boechler et al., 2011; Chong et al., 2017). Analytical methods for such granular systems primarily focus on reduced-order linearized approximations. In most such investigations, the discrete nature of the system is ignored, and the system is analyzed in the continuum limit. However, such analysis fails to capture nonlinear phenomena that emerge from the non-integrable discreteness in the system and the response can diverge significantly from the predictions (Somfai et al., 2005; Nesterenko et al., 2005). Therefore, there is currently no general systematic methodology for studying the temporal and spatial characteristics of the wave response in disordered granular crystals and designing materials with the desired dynamic response (Ganesh & Gonella, 2017).

In this paper, we develop a differentiable simulator for granular materials that can be incorporated into an optimization pipeline to find the best material properties to perform mechanical computations. Appendix A provides a summary of related works.

2. Methods

Figure 1 presents an overview of the optimization framework. A dense packing of circular particles with different material properties is subjected to external mechanical vibrations by displacing the selected input particle(s) with a predefined oscillatory force indicated as $X(t)$. The system's hidden state ($h_t = (r, \dot{r})_t$) can be described with the position (r_t) and velocity ($\dot{r}_t$) of the particles in time. In the forward pass, the system's state evolves according to the dynamics dictated by the physical system and depends on the state in the previous time step (h_{t-1}), physical parameters (θ), and the input at time t (X_t). The physics model describes the nonlinear relation between the state, input, and the parameters as $h_t = f(\theta, h_{t-1}, X_t)$. This is analogous to Recurrent Neural Networks (RNNs), where the hidden state allows the network to remember the past information fed into the network and enables learning of the temporal structure and long dependencies in the input. The output is defined as the measurements of a physical property of the system in time such as the displacement of the chosen output particle(s) $\hat{Y}_t$. To train the physical network, we need to update the trainable parameters θ, which are the mate-
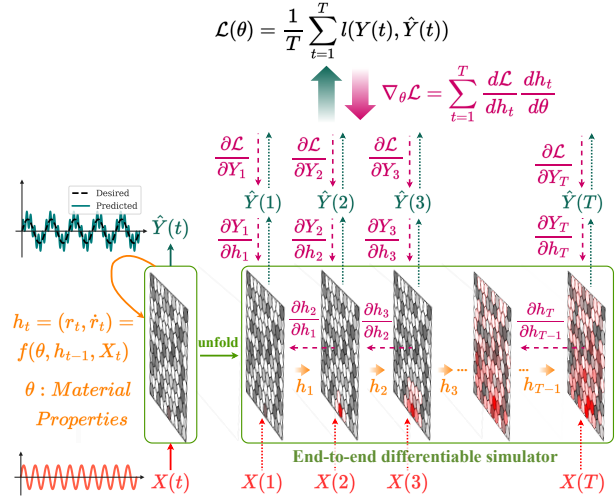

Figure 1. Inverse design of computational granular crystals. When the granular crystal is vibrated at its boundary, the elastic compression waves (indicated by the red shades in the panels) propagate in the material until they are scattered or attenuated by disorder, affected by dispersion, or distorted by (self-)demodulation and frequency mixing at nonlinear interparticle contacts (*Forward Pass*). The waves arriving at the output particle(s) are recorded and the difference between the desired ($Y(t)$) and recorded response ($\hat{Y}(t)$) is utilized in a loss function ($\mathcal{L}$) to adjust the trainable parameters (θ). f relates the input X_t, parameters θ, and the hidden state of the system h_{t-1} to the hidden state at the next time step h_t. An end-to-end differentiable physics simulator allows us to track the partial derivatives in the *Backward Pass* indicated by the pink arrows in the figure. The particles' material properties can be optimized with a gradient-based method to produce the desired nonlinear wave response.

rial properties of the particles (equivalent to weights of an RNN), to reduce the loss $\mathcal{L}$ defined between the real $\hat{Y}_t$ and desired $Y(t)$ outputs over T time steps.

An end-to-end differentiable simulator allows us to retain the gradients of the loss function with respect to the trainable parameters ($\nabla_\theta \mathcal{L}$) to be used in backpropagation. Similar to traditional RNNs, the gradients are obtained by taking the partial derivatives and using the chain rule as follows:

$$
\begin{aligned}
\nabla_\theta \mathcal{L} &= \sum_{t=1}^{T} \frac{d\mathcal{L}}{dh_t} \frac{dh_t}{d\theta} \\
\frac{d\mathcal{L}}{dh_t} &= \frac{\partial \mathcal{L}}{\partial h_t} + \frac{\partial \mathcal{L}}{\partial h_{t+1}} \frac{\partial h_{t+1}}{\partial h_t} \\
\frac{\partial \mathcal{L}}{\partial h_t} &= \frac{\partial \mathcal{L}}{\partial Y_t} \frac{\partial Y_t}{\partial h_t} \\
\frac{dh_t}{d\theta} &= \frac{\partial f}{\partial \theta}
\end{aligned}
\tag{1}
$$

Having the gradients of the loss function with respect to the physical parameters of the network, a gradient-based optimization method can be used to update the parameters (θ) at time step T and start the next forward pass.

2.1. Differentiable Simulator

Figure 2 shows an overview of the granular crystals we aim to optimize in this work. Deformable spherical particles with identical diameters and various elasticity are placed on a hexagonal lattice with fixed boundaries in both x and y directions. In this system, the repulsive force between two neighboring particles is nonlinear and can be described by the Hertz law (Hertz, 1882). More details about the physics model are provided in Appendix B.
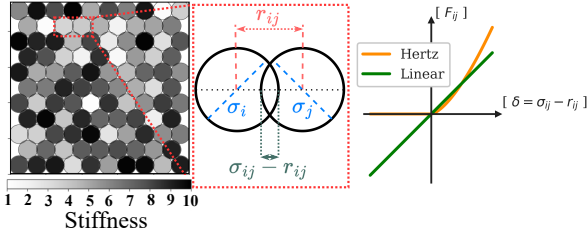

Figure 2. A granular crystal is made of spherical particles with identical size (diameter σ) and various stiffnesses (represented in different shades of grey) in a confined configuration with fixed boundaries. *Hertz's law* describes the relation between the particle's overlap ($\delta = \sigma_{ij} - r_{ij}$) and applied force ($F$) as $F = \alpha \delta^{\beta}$. Here, β is a constant that depends on the particle geometry and determines the nonlinearity of the contact forces. A commonly used value for spherical contacts is $\beta = \frac{3}{2}$, which produces a cubic nonlinearity in the equations of motion. $r_{ij} = |r_i - r_j|$ is the interparticle distance and $\sigma_{ij} = \frac{\sigma_i + \sigma_j}{2}$ is the maximum distance, after which the particles lose contact. As it is shown in the plot on the right, the interparticle potential is one-sided, and unlike a Hookean spring, the force becomes zero when the two particles lose contact.

Discrete Element Method (DEM) (Cundall & Strack, 1979) can be used to numerically simulate the motion of the interacting particles in a granular crystal. In this paper, we developed a differentiable simulator with the same method (details available in Appendix B.3) in the *PyTorch* framework (Paszke et al., 2017).

2.2. Optimization Setup

When a disordered granular crystal, such as the one shown in Figure 2, is vibrated at its boundaries, the produced elastic waves propagate through the material and scatter at the particle-particle interfaces. The material properties of the individual particles (elasticity, density, etc.), their geometry (shapes and sizes), and their arrangement (neighboring contact points) determine the distortion of the elastic waves and their frequency and amplitude-dependent attenuation. In this paper, we formulate the optimization problem of finding the stiffness values of the particles in a hexagonal granular crystal to achieve a desired wave response. Therefore, the trainable parameters, as defined in Equation (1), are $\theta = k_i, i \in [0, N]$ where N is the total number of the particles. The desired wave response is defined in terms of the displacement of the selected output particles and formulated

into the loss function $\mathcal{L}$ for the optimization.

2.3. Gradient-based Optimization

To enable the gradient-based optimization of granular crystals, we used PyTorch's automatic differentiation (*autodiff*) engine to compute the gradients of the loss function with respect to the trainable material properties (θ). We implemented custom submodules for the granular crystal simulation. Adam optimizer (Kingma & Ba, 2017) with an adaptive learning rate is utilized for the training process.

3. Experiments

To demonstrate the application of our gradient-based design framework we considered three design problems, including an acoustic waveguide (Appendix C), a mechanical AND gate, and a mechanical XOR gate (Appendix D). The detailed description of the simulation and model parameters is presented in Appendix B.
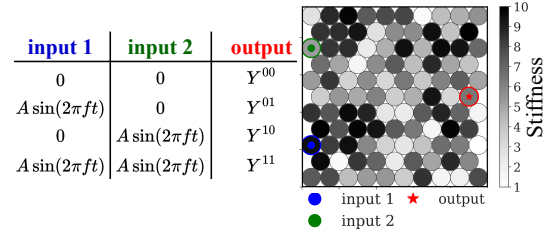
3.1. Acoustic Logic Gate

Figure 3. Experimental setup for the acoustic logic gates. The granular crystal is made of circular particles with various stiffness values represented in different shades of grey. The two particles on the left (with green and blue markers) are selected as the input ports where the external sinusoidal oscillations are applied to the system. As noted in the truth table, the 0/1 values at the ports are encoded as harmonic vibrations at a particular frequency f. The **00** case has a trivial solution that is always correct: since there are no power sources in the system, the lack of input vibrations means the output is 0, which is true for both AND and XOR gates. For the other three cases (**01**, **10**, and **11**) the horizontal displacement of the output particle from its equilibrium position ($r^x(t)$) is measured to infer the output of the logic function.

To demonstrate the computational capabilities of new physical substrates as alternatives to traditional digital electronics, many studies show designs for basic logic gates as a reasonable benchmark (Yasuda et al., 2021). In this paper, we first showed the design of an acoustic AND gate. To showcase the exploitation of the nonlinear dynamics of granular crystals for mechanical computing, we also investigated the design of an XOR gate as it performs a nonlinear input-output transformation. Figure 3 shows our experimental setup for the realization of acoustic logic gates.

The input and output signals are mechanical vibrations of the selected particles in the granular crystals. To design

logic functions, we first need to define a representation relation that dictates how we encode the binary values. Here, we measure the horizontal displacement of the particles from their equilibrium positions: using the amplitude of the input vibration as the baseline, a significant periodic displacement is interpreted as the binary 1 value, and a negligible one is interpreted as 0. We apply sinusoidal vibrations as the input and for the experiments in this section, we fixed the operational frequency of the logic gate at a predetermined frequency ($f = 15[Hz]$), which was chosen according to the material properties of the granular crystal and its frequency spectrum. The amplitude of oscillations (A) is fixed at a value of 10^{-3}.

To tune the particles' stiffness values, we define the *L-1* loss function (Mean Absolute Error, MAE) between the intensity of the horizontal displacement of the output particle ($\hat{Y} = [r_{output}^x(t)]_{t=\frac{2T}{3}}^{T}$) and the desired output (Y) as follows:

$$\mathcal{L}_{MAE}(Y, \hat{Y}) = \parallel Y - \hat{Y} \parallel_{MAE}$$
$$= \frac{1}{N} \sum_{n=1}^{N} |(Y^n - \hat{Y}^n| \qquad (2)$$

where N is the number of samples in the training dataset D, and the superscript n represents the output for each sample. When calculating the wave intensity, we only use the last one-third of the simulation time ($[\frac{2T}{3}, T]$, where T is the total simulation) to ignore the transient part of the signals.

3.2. AND Gate

We start with designing an AND gate because, due to its linear nature, we expect the design process to be straightforward. Although, due to the strong nonlinearity in the system, the material is theoretically capable of more complex computations, the high-dimensional parameter space (10×11 real numbers in $[1.0, 10.0]$) can make the gradient-based optimization challenging. The training dataset D is made of time series for the three binary input cases as follows:

$$D = \{$$
$$(X^{01} = [X_1 = A \sin 2\pi f t, X_2 = 0]_{t=1}^{T}, Y^{01} = [0]_{t=1}^{T}),$$
$$(X^{10} = [X_1 = 0, X_2 = A \sin 2\pi f t]_{t=1}^{T}, Y^{10} = [0]_{t=1}^{T}),$$
$$(X^{11} = [X_1 = A \sin 2\pi f t, X_2 = A \sin 2\pi f t]_{t=1}^{T},$$
$$Y^{11} = [A \sin 2\pi f t]_{t=1}^{T})\} \qquad (3)$$

Figure 4 presents the training loss and an example of the optimized material from one of the 10 independent trials in each of the two setups. It should be noted that the sudden changes in the training loss at specific instances are due to the incorporation of an adaptive learning rate. We incorporated a multi-step adaptive learning rate with a decay rate of $\gamma = 0.1$ and step sizes at $[150, 300, 400]$ epochs for the fixed-value initialization and $[100, 200, 300]$ epochs for the
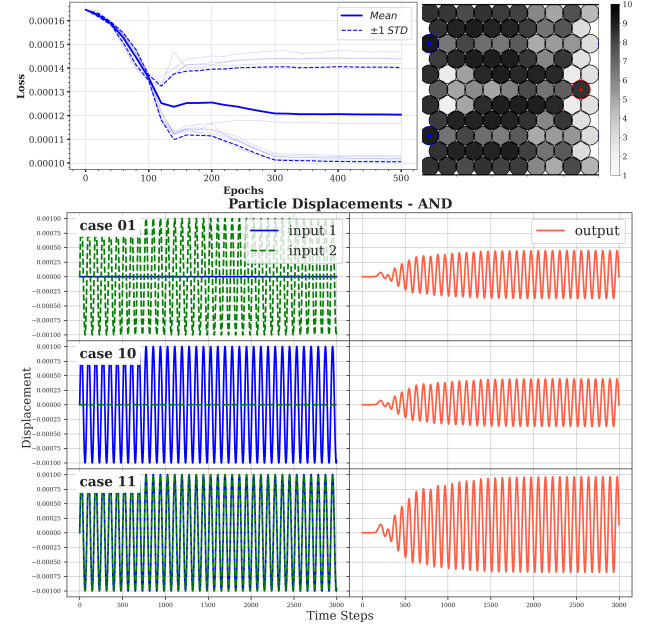

Figure 4. Gradient-based design of an acoustic AND gate. The granular crystal is initialized as a homogeneous assembly of particles with a stiffness value located in the middle of the permitted range. Each light graph in the top left panel shows the training loss for one of the 10 independent trials over 500 epochs. One example of the optimized material is shown on the right. The plots on the bottom show the inputs and output of the logic gate, as the horizontal displacement of the particles in time. Each row shows one of the three cases (**01**, **10**, and **11**).

randomly initialized case. The starting value of the learning rate is set to $lr = 0.001$ in both cases.

4. Conclusions

Motivated by the growing interest in unconventional computing substrates, we explored the application of gradient-based optimization frameworks for designing computational granular materials. We showed that by developing a differentiable simulator, we can employ gradient-based optimization to tune the material properties of the constituent particles of a granular crystal to allow for the desired wave responses.

Unlike previous work such as Mechanical Neural Networks that train the physical system directly (Lee et al., 2022), here we trained the physics model in a differentiable simulator. Therefore, transferring the designs to reality can be challenging because of the discrepancies between the real and simulated systems. In future work, we can address this by including random amounts of reasonable noise to the parameters and finding designs that tolerate reasonable manufacturing errors. Despite this, our approach can provide valuable insights into the design space of granular crystals. For example, using our design framework we can investigate which physical properties of the physical substrate offer more opportunities for a desired computational task.

References

Anderson, M. G., Ma, S.-Y., Wang, T., Wright, L. G., and McMahon, P. L. Optical Transformers, February 2023.

Asenjo-Andrews, D. A. *Direct Computation of the Packing Entropy of Granular Materials*. PhD thesis, University of Cambridge, 2013.

Boechler, N., Theocharis, G., and Daraio, C. Bifurcation-based acoustic switching and rectification. *Nature Materials*, 10(9):665–668, September 2011. ISSN 1476-4660. doi: 10.1038/nmat3072.

Chong, C., Porter, M. A., Kevrekidis, P. G., and Daraio, C. Nonlinear coherent structures in granular crystals. *Journal of Physics: Condensed Matter*, 29(41):413003, September 2017. ISSN 0953-8984. doi: 10.1088/1361-648X/aa7672.

Cui, J.-G., Yang, T., and Chen, L.-Q. Frequency-preserved non-reciprocal acoustic propagation in a granular chain. *Applied Physics Letters*, 112(18):181904, May 2018. ISSN 0003-6951. doi: 10.1063/1.5009975.

Cundall, P. A. and Strack, O. D. L. A discrete numerical model for granular assemblies. *Géotechnique*, 29(1):47–65, March 1979. ISSN 0016-8505, 1751-7656. doi: 10.1680/geot.1979.29.1.47.

Echeverri Restrepo, S., Sluiter, M. H. F., and Thijsse, B. J. Atomistic relaxation of systems containing plasticity elements. *Computational Materials Science*, 73:154–160, June 2013. ISSN 0927-0256. doi: 10.1016/j.commatsci.2013.03.001.

El Helou, C., Grossmann, B., Tabor, C. E., Buskohl, P. R., and Harne, R. L. Mechanical integrated circuit materials. *Nature*, 608(7924):699–703, August 2022. ISSN 1476-4687. doi: 10.1038/s41586-022-05004-5.

Eristoff, S., Kim, S. Y., Sanchez-Botero, L., Buckner, T., Yirmibeşoğlu, O. D., and Kramer-Bottiglio, R. Soft Actuators Made of Discrete Grains. *Advanced Materials (Deerfield Beach, Fla.)*, 34(16):e2109617, April 2022. ISSN 1521-4095. doi: 10.1002/adma.202109617.

Finocchio, G., Bandyopadhyay, S., Lin, P., Pan, G., Yang, J. J., Tomasello, R., Panagopoulos, C., Carpentieri, M., Puliafito, V., Åkerman, J., Takesue, H., Trivedi, A. R., Mukhopadhyay, S., Roy, K., Sangwan, V. K., Hersam, M. C., Giordano, A., Yang, H., Grollier, J., Camsari, K., Mcmahon, P., Datta, S., Incorvia, J. A., Friedman, J., Cotofana, S., Ciubotaru, F., Chumak, A., Naeemi, A. J., Kaushik, B. K., Zhu, Y., Wang, K., Koiller, B., Aguilar, G., Temporão, G., Makasheva, K., Sanial, A. T., Hasler, J., Levy, W., Roychowdhury, V., Ganguly, S., Ghosh, A., Rodriquez, D., Sunada, S., Evershor-Sitte, K., Lal, A.,

Jadhav, S., Di Ventra, M., Pershin, Y., Tatsumura, K., and Goto, H. Roadmap for Unconventional Computing with Nanotechnology, January 2023.

Franklin, S. V. and Shattuck, M. D. *Handbook of Granular Materials*. CRC Press, 2016.

Ganesh, R. and Gonella, S. Nonlinear waves in lattice materials: Adaptively augmented directivity and functionality enhancement by modal mixing. *Journal of the Mechanics and Physics of Solids*, 99:272–288, February 2017. ISSN 0022-5096. doi: 10.1016/j.jmps.2016.11.001.

Gao, G.-J., Blawzdziewicz, J., and O'Hern, C. S. Geometrical families of mechanically stable granular packings. *Physical Review E*, 80(6):061303, December 2009. doi: 10.1103/PhysRevE.80.061303.

Hertz, H. Ueber die Berührung fester elastischer Körper. 1882(92):156–171, January 1882. ISSN 1435-5345. doi: 10.1515/crll.1882.92.156.

Hughes, T. W., Williamson, I. A. D., Minkov, M., and Fan, S. Wave physics as an analog recurrent neural network. *Science Advances*, 5(12):eaay6946, December 2019. doi: 10.1126/sciadv.aay6946.

Huo, Y., Bao, H., Peng, Y., Gao, C., Hua, W., Yang, Q., Li, H., Wang, R., and Yoon, S.-E. Optical neural network via loose neuron array and functional learning. *Nature Communications*, 14(1):2535, May 2023. ISSN 2041-1723. doi: 10.1038/s41467-023-37390-3.

Jiang, J., Chen, M., and Fan, J. A. Deep neural networks for the evaluation and design of photonic devices. *Nature Reviews Materials*, 6(8):679–700, August 2021. ISSN 2058-8437. doi: 10.1038/s41578-020-00260-1.

Jiang, T., Li, T., Huang, H., Peng, Z.-K., and He, Q. Metamaterial-Based Analog Recurrent Neural Network Toward Machine Intelligence. *Physical Review Applied*, 19(6):064065, June 2023. doi: 10.1103/PhysRevApplied.19.064065.

Jiao, P., Mueller, J., Raney, J. R., Zheng, X. R., and Alavi, A. H. Mechanical metamaterials and beyond. *Nature Communications*, 14(1):6004, September 2023. ISSN 2041-1723. doi: 10.1038/s41467-023-41679-8.

Kadic, M., Milton, G. W., van Hecke, M., and Wegener, M. 3D metamaterials. *Nature Reviews Physics*, 1(3):198–210, March 2019. ISSN 2522-5820. doi: 10.1038/s42254-018-0018-y.

Karuriya, A. N. and Barthelat, F. Granular crystals as strong and fully dense architectured materials. *Proceedings of the National Academy of Sciences*, 120(1):e2215508120, January 2023. doi: 10.1073/pnas.2215508120.

Kingma, D. P. and Ba, J. Adam: A Method for Stochastic Optimization, January 2017.

Lawney, B. P. and Luding, S. Frequency filtering in disordered granular chains. *Acta Mechanica*, 225(8):2385–2407, August 2014. ISSN 0001-5970, 1619-6937. doi: 10.1007/s00707-014-1130-4.

Lee, R. H., Mulder, E. A. B., and Hopkins, J. B. Mechanical neural networks: Architected materials that learn behaviors. *Science Robotics*, 7(71):eabq7278, October 2022. doi: 10.1126/scirobotics.abq7278.

Li, F., Anzel, P., Yang, J., Kevrekidis, P. G., and Daraio, C. Granular acoustic switches and logic elements. *Nature Communications*, 5(1):5311, October 2014. ISSN 2041-1723. doi: 10.1038/ncomms6311.

Mao, S., Cheng, L., Zhao, C., Khan, F. N., Li, Q., and Fu, H. Y. Inverse Design for Silicon Photonics: From Iterative Optimization Algorithms to Deep Neural Networks. *Applied Sciences*, 11(9):3822, January 2021. ISSN 2076-3417. doi: 10.3390/app11093822.

Nakajima, K. Physical reservoir computing – An introductory perspective. *Japanese Journal of Applied Physics*, 59(6):060501, June 2020. ISSN 0021-4922, 1347-4065. doi: 10.35848/1347-4065/ab8d4f.

Nakajima, M., Inoue, K., Tanaka, K., Kuniyoshi, Y., Hashimoto, T., and Nakajima, K. Physical deep learning with biologically inspired training method: Gradient-free approach for physical hardware. *Nature Communications*, 13(1):7847, December 2022. ISSN 2041-1723. doi: 10.1038/s41467-022-35216-2.

Nesterenko, V. F., Daraio, C., Herbold, E. B., and Jin, S. Anomalous Wave Reflection at the Interface of Two Strongly Nonlinear Granular Media. *Physical Review Letters*, 95(15):158702, October 2005. doi: 10.1103/PhysRevLett.95.158702.

Papp, Á., Porod, W., and Csaba, G. Nanoscale neural network using non-linear spin-wave interference. *Nature Communications*, 12(1):6422, November 2021. ISSN 2041-1723. doi: 10.1038/s41467-021-26711-z.

Parsa, A., Witthaus, S., Pashine, N., O'Hern, C., Kramer-Bottiglio, R., and Bongard, J. Universal Mechanical Polycomputation in Granular Matter. In *Proceedings of the Genetic and Evolutionary Computation Conference*, GECCO '23, pp. 193–201, New York, NY, USA, July 2023. Association for Computing Machinery. ISBN 9798400701191. doi: 10.1145/3583131.3590520.

Paszke, A., Gross, S., Chintala, S., Chanan, G., Yang, E., DeVito, Z., Lin, Z., Desmaison, A., Antiga, L., and Lerer, A. Automatic differentiation in PyTorch. October 2017.

Pishvar, M. and Harne, R. L. Foundations for Soft, Smart Matter by Active Mechanical Metamaterials. *Advanced Science*, 7(18):2001384, 2020. ISSN 2198-3844. doi: 10.1002/advs.202001384.

Porter, M. A., Kevrekidis, P. G., and Daraio, C. Granular crystals: Nonlinear dynamics meets materials engineering. *Physics Today*, 68(LA-UR-15-21727), November 2015. ISSN 0031-9228. doi: 10.1063/PT.3.2981.

Rafsanjani, A., Bertoldi, K., and Studart, A. R. Programming soft robots with flexible mechanical metamaterials. *Science Robotics*, 4(29):eaav7874, April 2019. doi: 10.1126/scirobotics.aav7874.

Roberts, N. and Adamatzky, A. Mining logical circuits in fungi. *Scientific Reports*, 12(1):15930, September 2022. ISSN 2045-2322. doi: 10.1038/s41598-022-20080-3.

Somfai, E., Roux, J.-N., Snoeijer, J. H., van Hecke, M., and van Saarloos, W. Elastic wave propagation in confined granular systems. *Physical Review E*, 72(2):021301, August 2005. doi: 10.1103/PhysRevE.72.021301.

Spadoni, A. and Daraio, C. Generation and control of sound bullets with a nonlinear acoustic lens. *Proceedings of the National Academy of Sciences*, 107(16):7230–7234, April 2010. doi: 10.1073/pnas.1001514107.

Taghizadeh, K., Steeb, H., and Luding, S. Energy propagation in 1D granular soft-stiff chain. *EPJ Web of Conferences*, 249:02002, 2021. ISSN 2100-014X. doi: 10.1051/epjconf/202124902002.

Tahersima, M. H., Kojima, K., Koike-Akino, T., Jha, D., Wang, B., Lin, C., and Parsons, K. Deep Neural Network Inverse Design of Integrated Photonic Power Splitters. *Scientific Reports*, 9(1):1368, February 2019. ISSN 2045-2322. doi: 10.1038/s41598-018-37952-2.

Verlet, L. Computer "Experiments" on Classical Fluids. I. Thermodynamical Properties of Lennard-Jones Molecules. *Physical Review*, 159(1):98–103, July 1967. doi: 10.1103/PhysRev.159.98.

Wright, L. G., Onodera, T., Stein, M. M., Wang, T., Schachter, D. T., Hu, Z., and McMahon, P. L. Deep physical neural networks trained with backpropagation. *Nature*, 601(7894):549–555, January 2022. ISSN 1476-4687. doi: 10.1038/s41586-021-04223-6.

Xia, X., Spadaccini, C. M., and Greer, J. R. Responsive materials architected in space and time. *Nature Reviews Materials*, 7(9):683–701, September 2022. ISSN 2058-8437. doi: 10.1038/s41578-022-00450-z.

Yao, K., Unni, R., and Zheng, Y. Intelligent nanophotonics: Merging photonics and artificial intelligence at the

nanoscale. *Nanophotonics*, 8(3):339–366, March 2019. ISSN 2192-8614. doi: 10.1515/nanoph-2018-0183.

Yasuda, H., Buskohl, P. R., Gillman, A., Murphey, T. D., Stepney, S., Vaia, R. A., and Raney, J. R. Mechanical computing. *Nature*, 598(7879):39–48, October 2021. ISSN 1476-4687. doi: 10.1038/s41586-021-03623-y.

Zhang, Y., Moore, K. J., McFarland, D. M., and Vakakis, A. F. Targeted energy transfers and passive acoustic wave redirection in a two-dimensional granular network under periodic excitation. *Journal of Applied Physics*, 118(23): 234901, December 2015. ISSN 0021-8979, 1089-7550. doi: 10.1063/1.4937898.

A. Related Work

Physical computing has been an active research topic in recent years, and many attempts have been made to take inspiration from deep learning concepts and incorporate machine learning techniques in designing novel computational hardware. Physical Reservoir Computing (PRC) is one such direction where a physical system is exploited for computation by applying the inputs to a physical substrate, collecting the raw measurements, and only training a linear "readout" layer to match the desired outputs (Nakajima, 2020). Recently, Physical Neural Networks (PNNs) have been introduced in which the hardware's physical transformation is trained in a similar manner to DNNs to perform the desired computations. Here, unlike PRC, the system's input-output transformation is directly trained with an algorithm called physics-aware training (PAT) that enables backpropagation on physical input and output sequences (Wright et al., 2022). Optical Neural Networks are an example of PNNs, that propose running deep learning frameworks for any task, such as classification or natural language processing, directly on an optical hardware instead of a digital electronic one such as a GPU (Anderson et al., 2023; Huo et al., 2023). In PNNs, the mechanical properties of the physical system do not change during the training; instead, the applied physical input is tuned with backpropagation using a differentiable model of the system to achieve the desired input-output transformation. Training PNNs with BP has a couple of drawbacks such as needing accurate knowledge of the physical system and being unsuitable for online training. Direct feedback alignment (DFA) was developed to address this by omitting the need for layer-by-layer propagation of error. However, it still requires modeling and simulation of the physical system (Nakajima et al., 2022).

Mechanical Neural Networks (MNNs) are another type of physical network that, unlike the previous works, tune the mechanical properties of the physical system during training. Lee et al. have developed a framework where the stiffness values of interconnected beams in a lattice are tuned for desired bulk properties like shear and Young's modulus or mechanical behaviors such as shape morphing (2022). Similar works have been done for analog wave-based computing where a differentiable model is developed based on the finite difference discretization of the dynamical equations describing a scalar wave field in continuous elastic metamaterials (Hughes et al., 2019; Jiang et al., 2023). The same approach is utilized in (Papp et al., 2021) for designing computing devices with spin waves propagating in a magnetic thin film. Here, a magnetic field distribution is designed to steer the spin waves in order to achieve the desired behavior. However, the system is not trained in hardware; instead, the material is discretized into cells with various material properties, that are determined using an approximate differentiable simulator. Such an approximate model will not capture the full dynamical behavior in the strongly nonlinear regime. Moreover, after manufacturing the optimized design there are no methods for online adaptation of the structural parameters and therefore such physical substrates are more suitable for tasks where a system is trained once and then used for inference many times.

Granular metamaterials are particulate systems where the properties of the individual particles can be modified independently. Therefore they offer the opportunity to build reconfigurable multifunctional materials. While gradient-based optimization has been explored to a great extent in designing continuous photonic materials (Tahersima et al., 2019; Yao et al., 2019; Mao et al., 2021; Jiang et al., 2021), designing granular crystals with desired dynamic responses has not been explored. There exists an extensive body of research on granular materials dating back over 200 years. However, a general connection between their dynamic wave response and their constituents' shapes and material properties remains unknown. Moreover, analytical exploration of the parameter space of granular materials is infeasible without imposing simplifying assumptions and approximations. In this paper, we present a gradient-based optimization framework for designing granular crystals with desired dynamic wave responses.

B. Physics Model

The granular crystals discussed in this paper are finite-length two-dimensional configurations of spherical particles with identical diameters and variable elasticity placed on a horizontal flat surface (Figure 2). The system is a macroscopic scale granular system (particle sizes are in the millimeter-to-centimeter range), so the only forces acting on each particle are the finite-range repulsive interparticle contact forces. On the scale of particle contacts, we consider normal forces resulting from the adjacent particles' overlaps and ignore the tangential forces and particle rotations. With these assumptions, the local potential between each pair of particles i and j can be written as:

$$V_{ij}(r_{ij}) = \frac{\epsilon}{\alpha}(1 - \frac{r_{ij}}{\sigma_{ij}})^{\alpha}\Theta(1 - \frac{r_{ij}}{\sigma_{ij}}) \tag{4}$$

where ϵ is the characteristic energy scale, r_{ij} is the particles' separation, and σ_{ij} is the center-to-center separation at which

the particles are in contact without any deformation. In the case of spherical particles with diameters σ_i and σ_i we'll have: $\sigma_{ij} = \frac{\sigma_i + \sigma_j}{2}$. Θ in this equation is the Heaviside function, which ensures that the potential field is one-sided, meaning that the particles only affect their adjacent neighbors when they are overlapping:

$$\Theta(1 - \frac{r_{ij}}{\sigma_{ij}}) = \begin{cases} 0 & \frac{r_{ij}}{\sigma_{ij}} \geq 1 \\ 1 & \frac{r_{ij}}{\sigma_{ij}} < 1 \end{cases} \tag{5}$$

This is the simplest model for a granular crystal that neglects special aspects such as particles' rotation and alignment, which might be more important in higher dimensional experimental setups but are negligible in smaller scales. The separation between two spherical particles is computed based on their Cartesian coordinates as follows:

$$|r_{ij}| = |\vec{r_i} - \vec{r_j}| = \sqrt{x_{ij}^2 + y_{ij}^2} \tag{6}$$

In Equation (4), α determines the nonlinearity of the contact force. In this paper, we consider Hertzian ($\alpha = \frac{5}{2}$) contacts to provide enough nonlinearity in the physical substrate for performing the desired computations. Interparticle forces can be obtained by taking the derivative of the potential (V_{ij}) with respect to the displacement:

$$\begin{aligned} F_{ij} &= -\frac{\partial V_{ij}(r_{ij})}{\partial r_{ij}} \\ &= \frac{\epsilon}{\sigma_{ij}}(1 - \frac{r_{ij}}{\sigma_{ij}})^{\alpha-1}\Theta(1 - \frac{r_{ij}}{\sigma_{ij}})\frac{\partial r_{ij}}{\partial(x_{ij} \text{ or } y_{ij})} \end{aligned} \tag{7}$$

We assume that the particles have similar mass (m) but can have different stiffness values. In this case, ϵ can be calculated using the effective stiffness as follows:

$$\epsilon_{ij} = \begin{cases} k_i = k_j & : \text{if } k_i = k_j \\ \dfrac{k_i \times k_j}{k_i + k_j} & : \text{if } k_i \neq k_j \end{cases} \tag{8}$$

Using the above notation, we can write Newton's equations of motion as:

$$m_i \ddot{r}_i = F_i = \sum_{j=1, j\neq i}^{N} F_{ij} + F_{ext} \tag{9}$$

where the first term is the total force from the neighboring particles, and the second term is the system's external forces, which include the interaction force from the walls (in case of a fixed boundary condition) and the excitation applied to the system in the form of harmonic vibrations. Using Equation (7), we can obtain the partial forces in a one-dimensional system as:

$$\begin{aligned} F^x(r_{ij}) &= \frac{\epsilon_{ij}}{\sigma_{ij}}(1 - \frac{x_{ij}}{\sigma_{ij}})^{\alpha-1} \quad \Theta(1 - \frac{x_{ij}}{\sigma_{ij}}) \\ F_{iw}^x &= \frac{\epsilon}{\sigma_i/2}(1 - \frac{x_i - x_w}{\sigma_i/2})^{\alpha-1} \quad \Theta(1 - \frac{x_i - x_w}{\sigma_i}) \end{aligned} \tag{10}$$

where F_{iw}^x is the force between particle i and the wall placed at x_w. In a two-dimensional system, the forces are given by:

$$F^x(r_{ij}) = \frac{\epsilon_{ij}}{\sigma_{ij}}(1 - \frac{r_{ij}}{\sigma_{ij}})^{\alpha-1} \quad \frac{x_{ij}}{r_{ij}} \quad \Theta(1 - \frac{r_{ij}}{\sigma_{ij}})$$

$$F^y(r_{ij}) = \frac{\epsilon_{ij}}{\sigma_{ij}}(1 - \frac{r_{ij}}{\sigma_{ij}})^{\alpha-1} \quad \frac{y_{ij}}{r_{ij}} \quad \Theta(1 - \frac{r_{ij}}{\sigma_{ij}})$$

$$F_{iw}^x = \frac{\epsilon}{\sigma_i/2}(1 - \frac{x_i - x_w}{\sigma_i/2})^{\alpha-1} \quad \Theta(1 - \frac{x_i - x_w}{\sigma_i})$$

$$F_{iw}^y = \frac{\epsilon}{\sigma_i/2}(1 - \frac{y_i - y_w}{\sigma_i/2})^{\alpha-1} \quad \Theta(1 - \frac{y_i - y_w}{\sigma_i}) \tag{11}$$

B.1. Dissipation

To capture the dissipation effects in real granular crystals, we remove the Hamiltonian assumption and incorporate a dash-pot form of dissipation with a velocity-dependent functional form and characteristic constants for background, particle-particle, and particle-wall interactions. This adds extra terms to the equations of motion of each particle i (Equation (9)), and we'll have:

$$m_i \ddot{r}_i = F_i = \sum_{j=1, j \neq i}^{N} F_{ij} + \sum_{walls} F_{iw} - F_{ib} + F_{ext} \tag{12}$$

where m_i is the mass of particle i and the dissipation F_{ib} is:

$$F_{ib} = Bv_i$$
$$+ \sum_j B_{pp} v_{ij} \Theta(1 - \frac{r_{ij}}{\sigma_{ij}})$$
$$+ \sum_{walls} B_{pw} v_i \Theta(1 - \frac{r_i - r_w}{\sigma_i}),$$
$$v_i = \frac{\partial r_i}{\partial t}, \quad v_{ij} = v_i - v_j \tag{13}$$

The damping coefficients (B: background damping, B_{pp} particle-particle damping, and B_{pw} particle-wall damping) are usually determined by curve fitting in an experimental setup.

B.2. Strength of Nonlinearity

The discrete nature of the granular crystals makes it possible to tune the degree of nonlinearity in the system's dynamics. As was mentioned in the introduction, we study the particles in a confined space and under an initial static compression, which keeps the particles in place. By controlling the amount of precompression, the system can transition from a linear to a strongly nonlinear regime. To study this effect, we introduce the packing fraction as follows:

$$\phi = \frac{A_{part}}{A_{sys}} \tag{14}$$

where A_{part} is the sum of the area of the particles, and A_{sys} is the area of the system (the confining box). In this paper, we assume that the unforced system is mechanically stable and above the jamming state (ϕ_j, mechanical rigidity). Because of the initial precompression, the system will have a nonzero initial energy that depends on the amount of overlap between adjacent particles. To find the initial particle positions ($\delta_{0,i}$) and interparticle overlaps, an energy minimization algorithm is used, which will be explained in the next subsection.

B.3. Numerical Simulation

We use the Discrete Element Method (DEM) (Cundall & Strack, 1979) to simulate the motion of the interacting particles in a granular crystal. The simulation starts with the initial configuration and updates the positions and velocities by numerically

integrating the equations of motion (Equation (9)). Since our granular packings are made of particles with various material properties and are initially compressed with a uniform force, we need to ensure that the initial configuration is statically stable (the ground state $u = 0$ and $\dot{u} = 0$ is the minimum of energy). Here, we adopt a packing generation protocol that applies successive compression/decompression by changing the particle sizes (Gao et al., 2009; Franklin & Shattuck, 2016). An energy minimization technique, Fast Inertial Relaxation Engine (FIRE) (Echeverri Restrepo et al., 2013), is used to relax the interparticle forces and reach equilibrium following the repetitive deformations. With this method, we can find the particles' initial positions for a mechanically stable configuration with a given boundary condition (Asenjo-Andrews, 2013). To integrate the equations of motion, we use the Velocity Verlet integration algorithm, which is derived by the Taylor expansion of the particle positions at a small period Δt around time t (Verlet, 1967).

B.4. Simulation Parameters

Table 1 includes the parameter values for the physics model and numerical simulations used in the experiments.

Table 1. Simulation parameters.

PARAMETER	VALUE
TOTAL TIME (T)	3×10^3
TIME STEP (Δt)	5×10^{-3}
LATTICE SIZE ($N = N_x \times N_y$)	10×11
MASS (m)	1.0
STIFFNESS (k)	$\in [1.0, 10.0]$
PACKING FRACTION (ϕ)	0.1
DIAMETER (σ)	0.1
BACKGROUND DAMPING (B)	1.0
PARTICLE-PARTICLE DAMPING (B_{pp})	0.0
PARTICLE-WALL DAMPING (B_{pw})	0.0

C. Acoustic Waveguide

Granular crystals have a discrete band structure with a high *cut-off frequency* that depends on the particle properties (size, Young modulus, and Poisson ratio), boundary conditions, and the applied longitudinal static stress (Franklin & Shattuck, 2016). In a harmonically driven system, only waves with frequencies within the pass band can propagate, and waves above the cut-off frequency are attenuated significantly. This phenomenon provides the opportunity to design granular crystals with desired band gaps and tunable filtering behavior that act as acoustic filters and waveguides (Spadoni & Daraio, 2010), acoustic switches and logic gates (Li et al., 2014). In an acoustic waveguide, the vibrational energy is localized toward specific locations. In the first experiment, we demonstrate how the dynamics of a granular crystal can be tuned by changing the particles' stiffnesses to selectively direct acoustic waves toward one of the two output particles based on the frequency content of the input signal. Figure 5 presents the setup for this experiment. A particle near the left boundary is selected as the input port where the acoustic vibration is injected into the system. The input vibration is in the form of a horizontal sinusoidal wave that displaces particle i from its equilibrium position ($\delta_{0,i}$, see Appendix B) such that $r_i^x(t) = \delta_{0,i} + A \sin \omega t$, where A is the amplitude of the input oscillation, and $\omega = 2\pi f$ is its frequency. Similar to the input port, two particles are chosen near the right boundary as the output ports. The horizontal displacements of these output particles are recorded during the simulation, and the wave intensity is calculated as follows:

$$\hat{Y}_i = \sum_{t=\frac{T}{3}}^{T} \left(r_i^x(t) \right)^2 \quad , i \in 1, 2 \tag{15}$$

where $r_i^x(t)$ is the displacement of the particle in x direction at time t, T is the length of the simulation and i indicates the particle index which is 1 or 2, representing one of the two output ports. To remove the effect of transient responses, the first one-third of the simulation time is not included in calculating the wave intensity. The predicted output of the physical neural network is a vector with two scalar values which are the normalized wave intensities at each of the output ports as $\hat{Y}^n = [\frac{\hat{Y}_1^n}{\hat{Y}_1^n + \hat{Y}_2^n}, \frac{\hat{Y}_2^n}{\hat{Y}_1^n + \hat{Y}_2^n}]$. n indicates the sample from the training dataset which has two entities and is defined
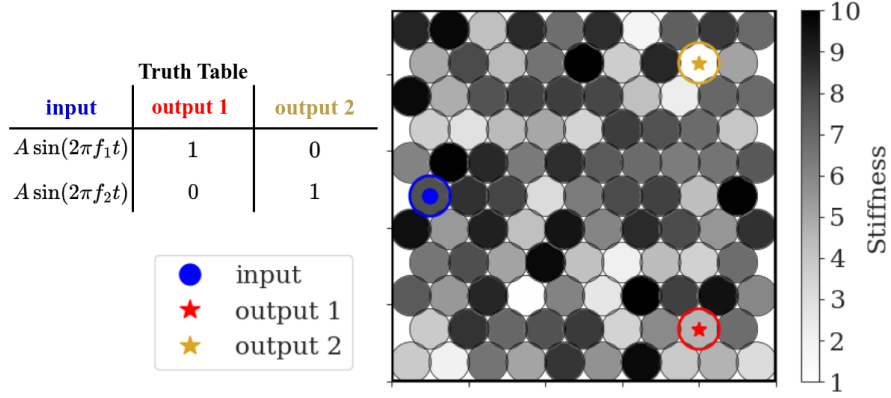
Figure 5. Experimental setup for the acoustic waveguide. The input particle (blue marker) is harmonically vibrated with the amplitude A and one of the two predefined frequencies, f_1 or f_2. The applied elastic vibrations propagate through the material, toward the output ports (red and gold markers). The existence of the input frequency in the displacement signal of the output particles indicates the computational response. Each of the two output particles is expected to only respond to one of the two input frequencies.

as $D = \{(X^1 = [A \sin 2\pi f_1 t]_{t=1}^T, Y^1 = [0,1]), (X^2 = ([A \sin 2\pi f_2 t]_{t=1}^T, Y^2 = [1,0])\}$. To tune the material with a gradient-based optimization framework, we defined a Cross-entropy (CE) loss as follows:

$$\mathcal{L}_{CE}(\hat{Y}, Y) = -\frac{1}{N} \sum_{n=1}^{N} \log \frac{exp(\hat{Y}_c^n)}{exp(\hat{Y}_1^n) + exp(\hat{Y}_2^n)}$$

$$c = argmax(Y^n) \tag{16}$$

where N is the size of the minibatch and c is the port index for the desired output for sample n from the minibatch. In
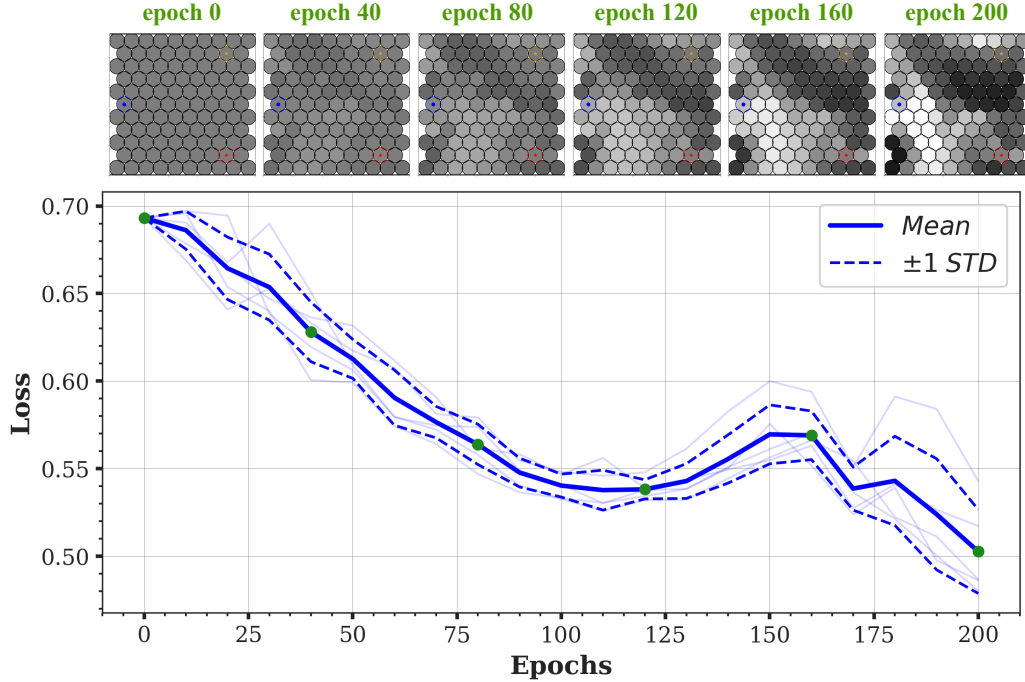

Figure 6. Inverse design of an acoustic waveguide. The training loss is plotted over 200 epochs. The mean and standard deviation of 5 independent runs are shown with solid and dashed lines respectively. Snapshots of the granular crystal are shown at intermediate stages during the training for one example trial.

this experiment, we applied small-amplitude vibrations to enforce the dynamics to stay in the weakly nonlinear regime

$(A = 10^{-2} \times \sigma = 10^{-3})$. The training dataset D consists of sinusoidal waves at two selected frequencies, $f_1 = 7[Hz]$, and $f_2 = 15[Hz]$. As mentioned before, one-hot encoding is utilized to indicate the desired output according to the truth table provided in Figure 6.

We initialized the stiffness profile (θ_0) with a stiffness value of $k = 5.0$ for all the particles at epoch 0 (see Figure 6). Adam optimizer is used with a fixed learning rate of 0.001 to train the network for 200 epochs. Figure 7 presents the training loss, averaged over 5 independent runs. As it can be seen in the optimized design at epoch 200 in Figure 7, the stiffness pattern of
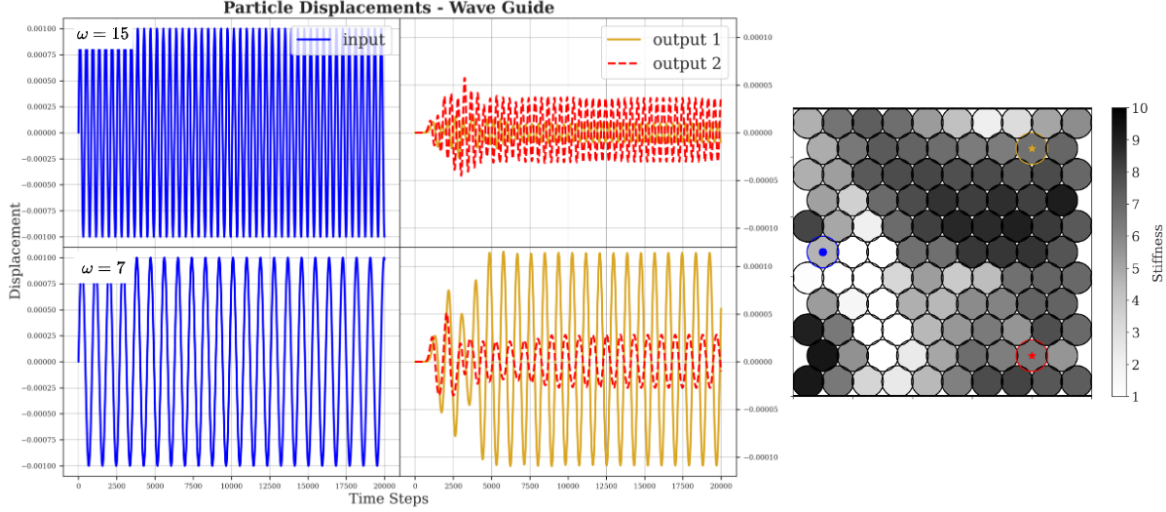

Figure 7. The optimized acoustic waveguide. The stiffness pattern enables the material to direct the vibration toward one of the output ports according to its frequency. The plots on the left show the horizontal displacement of the input (blue) and output particles (red and gold) during the simulation time. The optimized material directs the input vibration toward the top particle when the frequency is $f_1 = 7[Hz]$ and the bottom particle when the frequency is $f_1 = 15[Hz]$.

the granular crystal is tuned such that the low-frequency vibration is guided toward the top particle. On the other hand, the softer particles around the bottom port enable larger displacements around the second output port when the input is at a high frequency.

D. XOR Gate

We repeated the design problem for an XOR gate with the same set of parameters for the simulator and the optimizer. As in the previous section, a dataset containing the time series of the inputs and the target is produced and incorporated for optimizing the stiffness values of the particles as follows:

$$
\begin{aligned}
D = \{ & \\
& (X^{01} = [X_1 = A \sin 2\pi ft, X_2 = 0]_{t=1}^T, \\
& Y^{01} = [A \sin 2\pi ft]_{t=1}^T), \\
& (X^{10} = [X_1 = 0, X_2 = A \sin 2\pi ft]_{t=1}^T, \\
& Y^{10} = [A \sin 2\pi ft]_{t=1}^T), \\
& (X^{11} = [X_1 = A \sin 2\pi ft, X_2 = A \sin 2\pi ft]_{t=1}^T, \\
& Y^{11} = [0]_{t=1}^T) \}
\end{aligned}
\tag{17}
$$

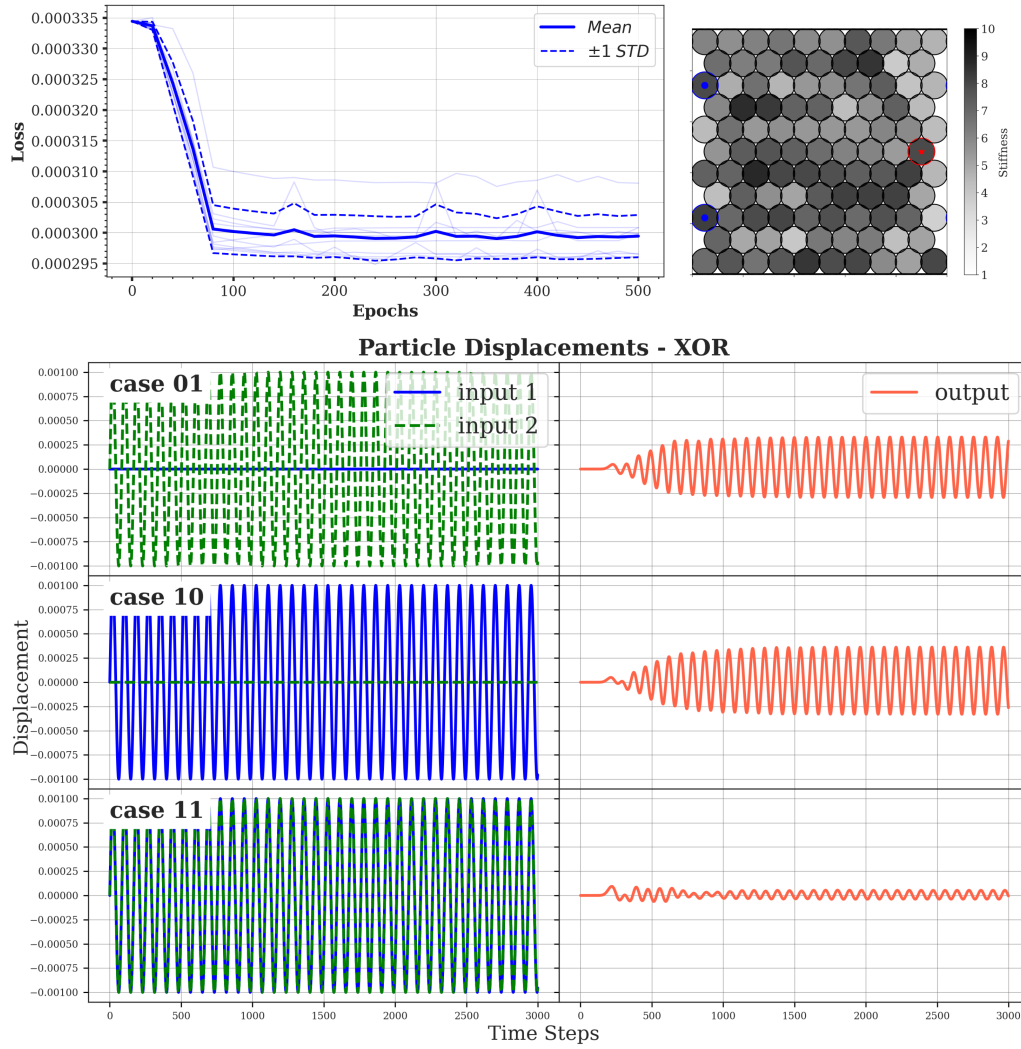The optimization results are shown in Figure 8.

Figure 8. Gradient-based design of an acoustic XOR gate. The granular crystal is initialized as a homogeneous assembly of particles with a stiffness value located in the middle of the permitted range. Each light graph in the top left panel shows the training loss for one of the 10 independent trials over 500 epochs. One example of the optimized material is shown on the right. The plots on the bottom show that, as we expect, the output particle oscillates with a higher amplitude when only one of the input ports is vibrated. This is consistent with the desired functionality of an XOR gate.